ORIGINAL ARTICLE

Journal of Cachexia, Sarcopenia and Muscle 2023; **14**: 1468–1481
Published online 20 April 2023 in Wiley Online Library (wileyonlinelibrary.com) **DOI:** 10.1002/jcsm.13234

Histopathological correlations and fat replacement imaging patterns in recessive limb-girdle muscular dystrophy type 12

Bram De Wel[1,2], Lotte Huysmans[3,4], Christophe E. Depuydt[2], Veerle Goosens[5], Ronald Peeters[5], Filipa P. Santos[2], Dietmar R. Thal[6,7], Patrick Dupont[8], Frederik Maes[3,4] & Kristl G. Claeys[1,2*]

[1]*Department of Neurology, University Hospitals Leuven, Leuven, Belgium;* [2]*Department of Neurosciences, Laboratory for Muscle Diseases and Neuropathies, KU Leuven, Leuven Brain Institute (LBI), Leuven, Belgium;* [3]*Medical Imaging Research Centre, University Hospitals Leuven, Leuven, Belgium;* [4]*Department ESAT - PSI, KU Leuven, Leuven, Belgium;* [5]*Department of Radiology, University Hospitals Leuven, Leuven, Belgium;* [6]*Department of Imaging and Pathology, Laboratory for Neuropathology, KU Leuven, Leuven Brain Institute (LBI), Leuven, Belgium;* [7]*Department of Pathology, University Hospitals Leuven, Leuven, Belgium;* [8]*Department of Neurosciences, Laboratory for Cognitive Neurology, KU Leuven, Leuven Brain Institute (LBI), Leuven, Belgium*

Abstract

Background Despite the widespread use of proton density fat fraction (PDFF) measurements with magnetic resonance imaging (MRI) to track disease progression in muscle disorders, it is still unclear how these findings relate to histopathological changes in muscle biopsies of patients with limb-girdle muscular dystrophy autosomal recessive type 12 (LGMDR12). Furthermore, although it is known that LGMDR12 leads to a selective muscle involvement distinct from other muscular dystrophies, the spatial distribution of fat replacement within these muscles is unknown.

Methods We included 27 adult patients with LGMDR12 and 27 age-matched and sex-matched healthy controls and acquired 6-point Dixon images of the thighs and T1 and short tau inversion recovery (STIR) MR images of the whole body. In 16 patients and 15 controls, we performed three muscle biopsies, one in the semimembranosus, vastus lateralis, and rectus femoris muscles, which are severely, intermediately, and mildly affected in LGMDR12, respectively. We correlated the PDFF to the fat percentage measured on biopsies of the corresponding muscles, as well as to the Rochester histopathology grading scale.

Results In patients, we demonstrated a strong correlation of PDFF on MRI and muscle biopsy fat percentage for the semimembranosus ($r = 0.85$, $P < 0.001$) and vastus lateralis ($r = 0.68$, $P = 0.005$). We found similar results for the correlation between PDFF and the Rochester histopathology grading scale. Out of the five patients with inflammatory changes on muscle biopsy, three showed STIR hyperintensities in the corresponding muscle on MRI. By modelling the PDFF on MRI for 18 thigh muscles from origin to insertion, we observed a significantly inhomogeneous proximo-distal distribution of fat replacement in all thigh muscles of patients with LGMDR12 ($P < 0.001$), and different patterns of fat replacement within each of the muscles.

Conclusions We showed a strong correlation of fat fraction on MRI and fat percentage on muscle biopsy for diseased muscles and validated the use of Dixon fat fraction imaging as an outcome measure in LGMDR12. The inhomogeneous fat replacement within thigh muscles on imaging underlines the risk of analysing only samples of muscles instead of the entire muscles, which has important implications for clinical trials.

Keywords Limb-girdle muscular dystrophy type R12; Muscle biopsy; MRI; Fat fraction; Fat replacement

Received: 12 September 2022; Revised: 13 February 2023; Accepted: 15 March 2023
**Correspondence to: Kristl Claeys, Department of Neurology, University Hospitals Leuven, Campus Gasthuisberg, Herestraat 49, 3000 Leuven, Belgium. Email:kristl.claeys@uzleuven.be*

Introduction

Fat fraction measured with quantitative MRI (qMRI) has been widely used to track disease progression in a range of muscle disorders for many years but MRI findings have only rarely been correlated to histopathological changes on muscle biopsies.[1–4] Dixon imaging is a frequently used MRI technique that divides all acquired voxels into either fat or water, which is a simplified representation of muscle histology.[5] Although a good correlation between fat fraction measurements on MRI and muscle biopsy is generally assumed, it is interesting to substantiate this for extra validation of the use of qMRI in clinical trials. In this study, we correlate the proton density fat fraction (PDFF) on MR imaging to the fat percentage measured on muscle biopsies of adult patients with limb-girdle muscular dystrophy autosomal recessive type 12 (LGMDR12). We also investigate whether short tau inversion recovery (STIR) hyperintensities coincide with inflammatory histopathological changes.

LGMDR12 is caused by bi-allelic pathogenic variants in the anoctamin-5 (*ANO5*) gene, resulting in slowly progressive proximal muscle weakness.[6] Recently, we showed that measurement of PDFF with qMRI was a useful outcome measure of disease progression in adult patients with LGMDR12.[7] We also demonstrated that PDFF values greatly varied between different measurement points along the length of thigh muscles in these patients.[7] An inhomogeneous distribution of PDFF along the length of thigh muscles has also been demonstrated in a few other neuromuscular diseases, such as in children with Duchenne muscular dystrophy (DMD) and adults with facioscapulohumeral muscular dystrophy.[8–11]

We further explore these findings by comprehensively modelling the distribution of muscle fat replacement from origin to insertion for 18 entire thigh muscles to demonstrate the variation in PDFF along the length of the muscles and search for muscle specific patterns of fat replacement in adult patients with LGMDR12 and age-matched and sex-matched healthy controls. This is crucial information, because in the current literature typically only a small, arbitrarily selected part of the muscles is analysed which can impose an important bias in the results.[7,8,12] As qMRI is increasingly being proposed as an outcome measure in clinical trials, it is highly relevant that it is analysed as accurately as possible; otherwise, false-negative or even false-positive findings with regard to new therapies might occur.[5,13–16] In addition, we explored the radial distribution of intramuscular fat from the outer edges to the centre of the muscles in order to gain a better understanding of the process of fat replacement in LGMDR12.

Patients and methods

Patients and study design

In this cross-sectional study, we included adult, ambulatory patients with genetically confirmed LGMDR12. All patients had to be symptomatic, which was defined as the presence of muscle weakness or myalgia and cramps. These criteria were chosen to improve phenotypic homogeneity and implied that patients with asymptomatic elevated serum creatine kinase (hyperCKemia) were not eligible to participate. For every patient an age-matched and sex-matched healthy control individual was included. Every participant underwent a whole-body muscle MRI and 6-point Dixon images of the entire upper legs and pelvis.

Biopsy technique and analysis

The muscle biopsy technique and procedure are described in more detail in a separate previous study, in which RNA-seq was performed on muscle tissue.[17] In short, following Dixon MRI of the thighs, a muscle biopsy of 2 cm in length was taken in three different muscles of patients with LGMDR12 and healthy controls: in the semimembranosus, vastus lateralis and rectus femoris. The median interval between MRI and biopsy was 5.5 days (range 1–66). The vacuum-assisted needle biopsies were performed under ultrasound guidance with the EnCor Enspire (breast) biopsy system and 10G EnCor needles (Bard Benelux, Olen, Belgium). Biopsies were immediately mounted on a separate cork, snap-frozen and stored at −80°C. Each biopsy was cut with a microtome-cryostat and samples from the proximal and distal parts of the biopsy were mounted on glass slides and evaluated under the microscope after haematoxylin and eosin staining.

We used ITK-SNAP to manually delineate fat tissue from muscle and connective tissue and calculated the biopsy fat percentage as the volume of fat tissue divided by the total volume of tissue in the biopsy image.[18] Additionally, one expert (KGC) calculated the histopathology grading scale of Rochester University to visually assess the severity of pathological changes in the biopsies of the patients.[1,19] This scale ranks four morphological characteristics (variability in fibre size, central nucleation, necrosis/regeneration, and interstitial fibrosis) on an ordinal scale between 0 and 3 (0 = normal; 1 = mild; 2 = moderate; and 3 = severe), producing a compound score of 0–12 points, and also scores the presence of inflammatory changes separately.

We correlated both the biopsy fat percentage and the histopathology grade to the PDFF measured on MRI of the

respective part of the muscles where the biopsy was taken. This was achieved by photographing the exact location of each muscle biopsy during the procedure. Next, using anatomical reference points, we measured the location of the muscle biopsy on the MRI images. As the length of the biopsy was 2 cm, we averaged the measured muscle PDFF over 2 cm (10 slices) at this location.

MRI data acquisition

We used a 1.5 Tesla Philips Ingenia MRI scanner (Philips Medical Systems, Best, the Netherlands) and acquired axial T1 turbo spin echo sequences (repetition time (TR) 412 ms, echo time (TE) 4.0 ms, 30 slices with 8 mm slice thickness and 1 mm interslice gap, field of view (FOV) 300 × 455 mm^2, voxel size = 1.4 × 1.4 mm^2) and coronal STIR images (repetition time (TR) 16 103 ms, echo time (TE) 70 ms, 45 slices with 6 mm slice thickness and 1 mm interslice gap, field of view (FOV) 371 × 550 × 314 mm^3, voxel size = 1.6 × 2.0 mm^2) of the whole body, and 6-point Dixon fast imaging in 3D of the thighs (TR/TE1/delta TE = 9.2/1.36/1.3 ms, flip angle (FA) 12°, 125 slices, slice thickness 2 mm, FOV 450 × 394 × 252 mm^3, matrix 320 × 280 × 125, voxel size 1.2 × 1.2 × 2 mm^3). These Dixon parameters were used because they are the standard mDixon_QUANT protocol of our Philips MRI scanner and they produce a good signal to noise ratio with a fast acquisition time at 1.5 T. However, given that a FA of 12° and a short TR incur T1-weighting in the Dixon images, we corrected for this in post-processing with the formulas described in Liu et al.[20] We acquired three Dixon imaging stacks from the iliac crest to the tibial plateau, each overlapping by 10 slices (20 mm).

MRI analysis

Due to the overlap of the three imaging stacks, we were able to exclude the peripheral five slices from each overlapping stack. This was done because B0 inhomogeneities frequently occur at the outer edges of MR images, which can affect the measured PDFF values. Next, we used a custom-made convolutional neural network (CNN) for semi-automated 3D segmentation of all imaging stacks.[21] This artificial intelligence supported workflow was described in detail in our recent study and represents a time-efficient and feasible way to obtain 3D segmentations of the entire thigh muscles.[7] Next, we calculated PDFF images out of the Dixon fat and water images as PDFF (%) = fat image/(fat + water image) with a custom-made MATLAB script (MathWorks, Natick, MA, USA). The script then utilized the 3D segmentations of each subject to calculate the mean PDFF per muscle per slice (of the left and right leg combined), which was used to evaluate the profile of muscle fat replacement along the length of the muscles from the most proximal slice to the most distal, along the *z*-axis of the images, as well as the mean PDFF per muscle.

Finally, we evaluated the radial profile of muscle fat replacement by calculating the mean PDFF of consecutive one-pixel wide layers from the outside to the centre of each muscle. For this analysis, we sampled a specific part of the muscle to avoid confounding of the radial profile with potential changes in PDFF along the length of the muscle: the slice with the maximal cross-sectional area (maxCSA) of the selected muscle and five proximal and five distal adjacent slices (over a total of 22 at 2 mm per slice). This section of the muscle was chosen because the CSA remains relatively stable over this rather short distance.

Statistical analysis

We used RStudio® Desktop (Open Source Licence, version 1.2.5001) for all statistical analyses. We calculated Spearman correlation coefficients and Bland–Altman plots to analyse the correlation between MRI and biopsy results. To investigate whether PDFF varied along the length of the muscles, we compared a non-linear mixed model with 3-knot bsplines with an intercept only mixed model, which assumed a homogeneous distribution of fat fraction along the length of the muscles for each patient. We used the Akaike information criterion (AIC) to compare these two models, as a lower AIC indicates a better model (a difference of >10 between models is considered significant).[22] Additionally, to aid in the interpretation of the results for those unfamiliar with the AIC, we performed an ANOVA likelihood ratio test to obtain a *P*-value for the comparison of these models. Although the ANOVA function is typically not used to compare these types of models (because it overestimates *P*-values), it is reliable in case significant *P*-values are found.[23]

The same technique was used to assess radial profiles. Additionally, we compared the average PDFF of the 50% most peripheral one-pixel wide layers to the 50% most inner layers of each muscle. A *t*-test or non-parametric alternative was used to compare groups. Holm's method was used to correct for multiple testing.[24]

Results

Patient characteristics

We included 27 adult LGMDR12 patients and 27 age-matched and sex-matched healthy controls, of which characteristics are detailed in Table 1. Median age at symptom onset was 30 years (range 8–52). All patients were ambulatory (three used walking aids), and the average six-minute walking distance (6MWD) was 549 ± 170 m. The mean Medical Research Council (MRC) sum score for manual muscle force grading

Table 1 Clinical and radiological characteristics of patients and controls

Demographics	Patients	Controls
Gender		
Male	22 (81.5%)	22 (81.5%)
Female	5 (18.5%)	5 (18.5%)
Current age (in years)	45 (21–72)	46 (24–71)
Disease duration (in years)	15 (1–35)	NA
PDFF %		
Semimembranosus	36.0 ± 33.4	7.6 ± 3.8
Biceps femoris long head	33.2 ± 32.5	6.6 ± 2.9
Adductor magnus	30.2 ± 26.6	5.7 ± 2.1
Adductor longus	25.9 ± 28.8	4.9 ± 1.7
Semitendinosus	23.0 ± 23.9	6.4 ± 2.1
Vastus medialis	22.8 ± 29.0	4.6 ± 1.9
Gluteus minimus	22.8 ± 20.0	8.6 ± 4.2
Tensor fascia lata	21.9 ± 20.1	10.1 ± 3.8
Vastus intermedius	20.5 ± 25.9	4.8 ± 1.7
Vastus lateralis	19.7 ± 25.1	5.1 ± 1.5
Biceps femoris short head	19.5 ± 21.2	6.8 ± 2.2
Gluteus maximus	17.7 ± 13.9	10.8 ± 4.5
Adductor brevis	15.1 ± 21.1	4.6 ± 1.1
Gracilis	12.7 ± 19.7	5.3 ± 1.5
Rectus femoris	12.3 ± 20.1	4.8 ± 1.3
Gluteus medius	11.6 ± 11.9	7.4 ± 2.0
Sartorius	11.2 ± 10.6	7.5 ± 2.7
Pectineus	7.7 ± 12.3	5.0 ± 1.2

Note: Data are shown as *n* (%), median (range) or as mean ± standard deviation.
Abbreviations: NA, not applicable; PDFF, proton density fat fraction.

was 56.6/60 ± 5.2 points. CK levels were elevated in all patients with an average of 2935 ± 2053 U/L. There were no patients with cardio-respiratory complications. Eight patients (30%) had a homozygous c.191dupA founder mutation in the *ANO5* gene and 10 (37%) were compound heterozygous for this pathogenic variant. The rest of the patients carried other *ANO5* variants. The average fat fraction of each muscle is shown in Table 1 for both the patient and control group. In general, thigh muscles in patients were affected symmetrically, with only 2/18 muscles showing an absolute side asymmetry of ≥5% PDFF that was significantly different from the physiological asymmetry in the control group (Table S1).

Correlation of MRI fat fraction measurements with histopathological findings in muscle biopsies

We biopsied the semimembranosus, vastus lateralis and rectus femoris muscles in 16 LGMDR12 patients and 15 healthy controls. We showed previously that specifically in patients with LGMDR12 these muscles are severely, moderately, and mildly affected, respectively, and hypothesized that this selection of muscles would provide a good overview of the range of histopathological changes.[7,17] For one patient and one control, biopsy data for the semimembranosus were missing due to technical issues.

For patients, we observed a moderately strong correlation of PDFF measurements on MRI and muscle biopsy fat fraction for the semimembranosus and vastus lateralis muscles, but not for the rectus femoris (Table 2). Note that fat fraction on MRI is consistently slightly higher than the fat percentage of biopsies in all three muscles, as evidenced by the tilted slope of the correlation lines (Figure 1, A1–3). A Bland–Altman analysis confirmed this and showed that this difference was the largest for the semimembranosus muscle in patients (Figure S1 and Table S2).

In the control group, we could not observe a significant correlation between PDFF and muscle biopsy fat percentage for the semimembranosus (ρ = 0.38, P = 0.202; PDFF 7.2 ± 2.9%, biopsy FF 3.4 ± 4.6%), vastus lateralis (ρ = 0.25, P = 0.368; PDFF 5.4 ± 1.3%, biopsy FF 2.3 ± 3.1%) and rectus femoris (ρ = −0.04, P = 0.883; PDFF 6.1 ± 1.6%, biopsy FF 1.4 ± 1.4%) muscles.

In patients, PDFF also strongly correlated to the histopathology grading scale for the semimembranosus and vastus lateralis muscles (Figure 1, B1–3). In 5/16 patients, we detected inflammatory changes in the muscle biopsies: in the vastus lateralis in three patients and in the semimembranosus in two. Of these patients, three showed STIR hyperintensities in the corresponding muscle (at the level of the biopsy) on MRI and one only in other leg muscles that were not biopsied. In 11/16 patients without inflammation on muscle biopsies, only one patient showed STIR hyperintensities, in other leg muscles that were not biopsied.

Proximo-distal profiles of muscle fat replacement in thigh muscles of patients and controls

We observed a significant inhomogeneous distribution of fat along the length of thigh muscles for each individual muscle

Table 2 Correlation of PDFF % MRI and muscle biopsy changes

	Correlation coefficients			
Muscles	Biopsy fat fraction %	*P*-value	Biopsy pathology grade	*P*-value
Semimembranosus PDFF %	0.85	<**0.001**	0.78	<**0.001**
Vastus lateralis PDFF %	0.68	**0.005**	0.77	<**0.001**
Rectus femoris PDFF %	0.17	0.530	0.18	0.516

Note: Spearman correlation coefficients are shown for the correlation between MRI measured PDFF of the respective muscles on the one hand and the fat fraction and Rochester University Histopathology Grade on muscle biopsy on the other hand. Significant *P*-values are marked in bold.
Abbreviations: MRI, magnetic resonance imaging; PDFF, proton density fat fraction.

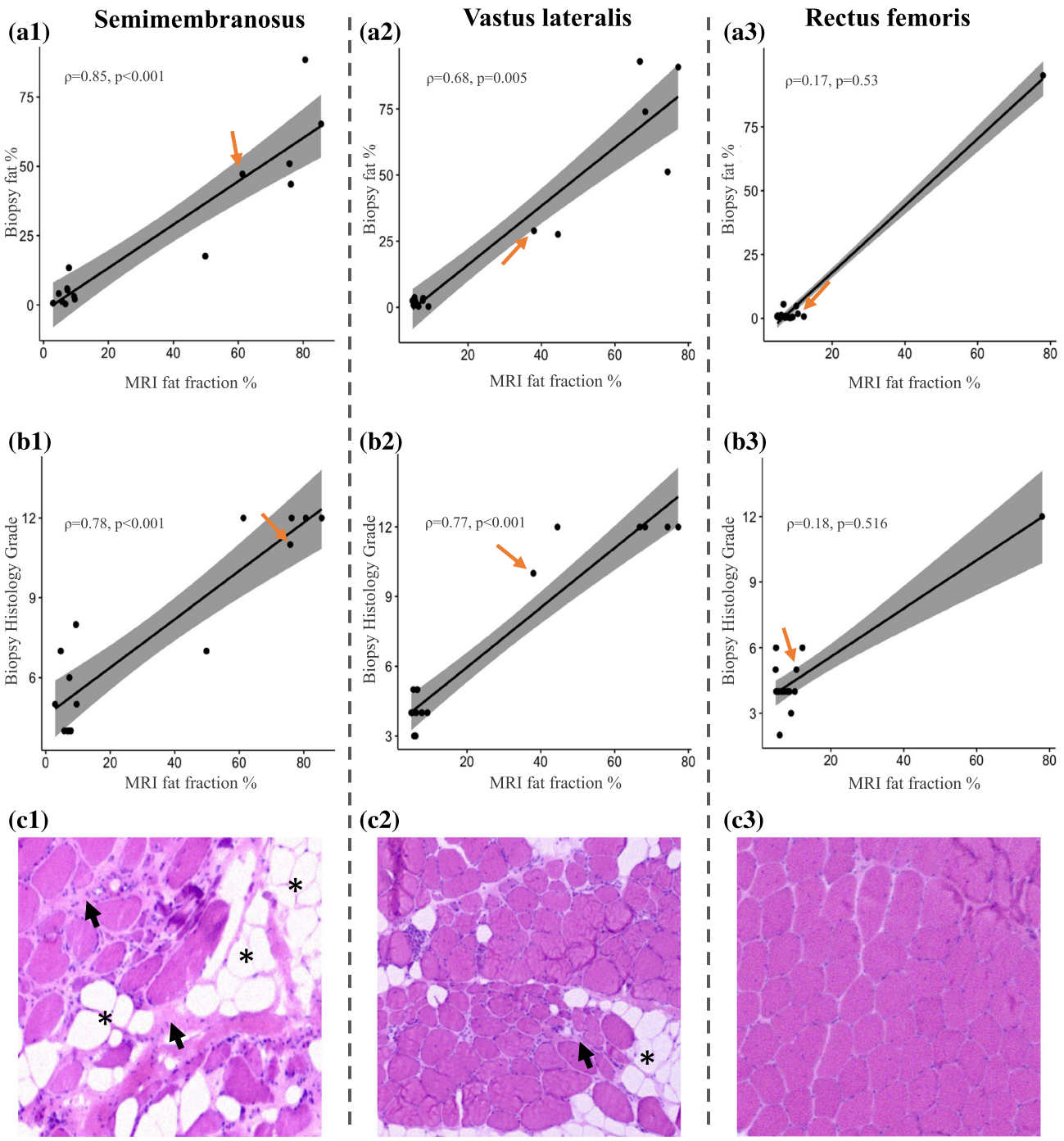

Figure 1 Correlation of PDFF on MRI with muscle biopsy fat percentage and histopathology grading scale. (A, B) There is a strong correlation between the fat fraction measured on MRI and both the fat percentage and severity of histopathological changes on biopsy of the corresponding area of the semimembranosus and vastus lateralis muscles, but not the rectus femoris. The orange arrows indicate the datapoints of the patient whose muscle biopsies are shown in row c. (C) Haematoxylin and eosin-stained muscle biopsy transverse sections of the respective muscles demonstrate the degree of histopathological changes within one patient: The semimembranosus is the most affected muscle (c1), the vastus lateralis is intermediately affected (c2) and the rectus femoris only mildly affected (c3). The biopsy images show increased fibre size variability, fatty tissue infiltration indicated by the asterisks, and fibrosis shown by the short black arrows. The biopsy images shown are purely for illustrative purposes and represent only a small portion of the analysed muscle tissue.

in both patients and controls with large differences in AIC with $P < 0.001$ for all muscles (Table 3, Figures 2 and 3). This confirmed that the PDFF was not equal in every slice along the length of the thigh muscles.

Upon visual inspection of the fat replacement profiles, we were able to discern different muscle-specific patterns that were followed by most patients, irrespective of their disease stage. For example, some muscles showed an upward facing parabola (e.g., vastus lateralis), with highest PDFF values at the origin and insertion of the muscles, and others a downward facing parabola (e.g., sartorius), with highest PDFF values at the centre of the muscle. Others still were best described with a cubic function (e.g., adductor magnus), with PDFF first increasing distally, and only in later disease stages more proximally. However, for some muscles, we did not observe a clear pattern of fat distribution followed by most patients or the pattern changed depending on disease stage. For example, the vastus intermedius muscle follows an upward facing parabola pattern in mildly affected patients, with a clearly distal predominant progression of muscle fat infiltration in the more severely affected, thereby following a cubic function pattern.

In the healthy control group PDFF values were within normal ranges as expected. However, all 18 investigated muscles also had an inhomogeneous distribution of PDFF along the length of the muscles, even though the differences in PDFF were very small (Table 3, Figure 4). The observed patterns in all the muscles of patients and controls are listed in Table 3 and visualized in Figures S2 and S3.

Radial profiles of muscle fat replacement in patients and controls

Along the radial axis, we also found an inhomogeneous distribution of fat for all muscles in patients and controls, but with very small changes in PDFF (Figures S4 and S5). There were generally no clear common patterns between patients, with a seemingly random fat replacement along the radial axis. Additionally, the average PDFF of the outer half of the muscles was not significantly different from the centre half for most muscles, with typically small effect sizes (Table 4). Although in some muscles (especially in the control group) there was a statistically significant difference, the mean differences along the radial axis were not significantly different

Table 3 Analysis of non-linearity and inhomogeneity of fat distribution over the length of thigh muscles

	Patients				Controls			
Muscles	AIC base model	AIC full model	*P*-value	Pattern	AIC base model	AIC full model	*P*-value	Pattern
Semimembranosus	1853	−3759	<**0.001**	Undefined	−1048	−4842	<**0.001**	Undefined
Biceps femoris long head	3910	−3430	<**0.001**	Undefined	−458	−5173	<**0.001**	Cubic *f*
Adductor magnus	9187	−577	<**0.001**	Cubic *f*	41	−3996	<**0.001**	Cubic *f*
Adductor longus	2445	−2799	<**0.001**	Cubic *f*	−876	−4546	<**0.001**	Cubic *f*
Semitendinosus	8139	−1014	<**0.001**	Cubic *f*	779	−3146	<**0.001**	Cubic *f*
Vastus medialis	5601	−2810	<**0.001**	Double	−1458	−6685	<**0.001**	U parabola
Gluteus minimus	3101	−341	<**0.001**	Cubic *f*	2702	−1410	<**0.001**	Cubic *f*
Tensor fascia lata	1817	−2130	<**0.001**	Cubic *f*	1922	−2915	<**0.001**	Cubic *f*
Vastus intermedius	6899	−5143	<**0.001**	Double	437	−7063	<**0.001**	U parabola
Vastus lateralis	5481	−4108	<**0.001**	U parabola	210	−6268	<**0.001**	U parabola
Biceps femoris short head	3905	−2633	<**0.001**	Cubic *f*	1728	−3336	<**0.001**	Cubic *f*
Gluteus maximus	6216	−4466	<**0.001**	Double	1007	−5045	<**0.001**	U parabola
Adductor brevis	3220	−1097	<**0.001**	Cubic *f*	−933	−2785	<**0.001**	Cubic *f*
Gracilis	3686	−2823	<**0.001**	Cubic *f*	264	−3997	<**0.001**	Cubic *f*
Rectus femoris	2873	−5251	<**0.001**	Undefined	2720	−6087	<**0.001**	Cubic *f*
Gluteus medius	3409	−2649	<**0.001**	Cubic *f*	1191	−3602	<**0.001**	Cubic *f*
Sartorius	7754	−1347	<**0.001**	∩ parabola	3928	−3367	<**0.001**	∩ parabola
Pectineus	253	−1459	<**0.001**	Undefined	−358	−2293	<**0.001**	Cubic *f*
Total all muscles	12476	−1039	<**0.001**	Undefined	4489	−10532	<**0.001**	Cubic *f*
Quadriceps muscle group	8692	−2824	<**0.001**	Double	−1530	−8824	<**0.001**	Cubic *f*
Adductor muscle group	9162	−1394	<**0.001**	Cubic *f*	−187	−5523	<**0.001**	Cubic *f*
Hamstrings muscle group	10 880	−1937	<**0.001**	∩ parabola	769	−4837	<**0.001**	∩ parabola

Note: The AIC was used to compare intercept only mixed models (base model), which assume a homogeneous distribution of fat fraction along the length of the muscles, with a non-linear mixed model modelling the measured fat fraction over the length of the muscles with 3-knot bsplines (full model; lower AIC indicates the better model). For all muscles of both patients and controls the non-linear bspline models were significantly superior at $P < 0.001$, which means that the measured fat fraction is not homogeneously distributed along the length of all the individual thigh muscles. We describe a rough pattern for proximo-distal fat replacement in each muscle that is followed by the majority of patients and controls: an upward facing parabola ('U parabola'), a downward facing parabola ('∩ parabola'), a cubic function ('Cubic *f*'), a 'double' pattern (changing with disease progression), and an 'undefined' pattern (with little coherence between subjects).
Abbreviation: AIC, Akaike information criterion.

DOI: 10.1002/jcsm.13234

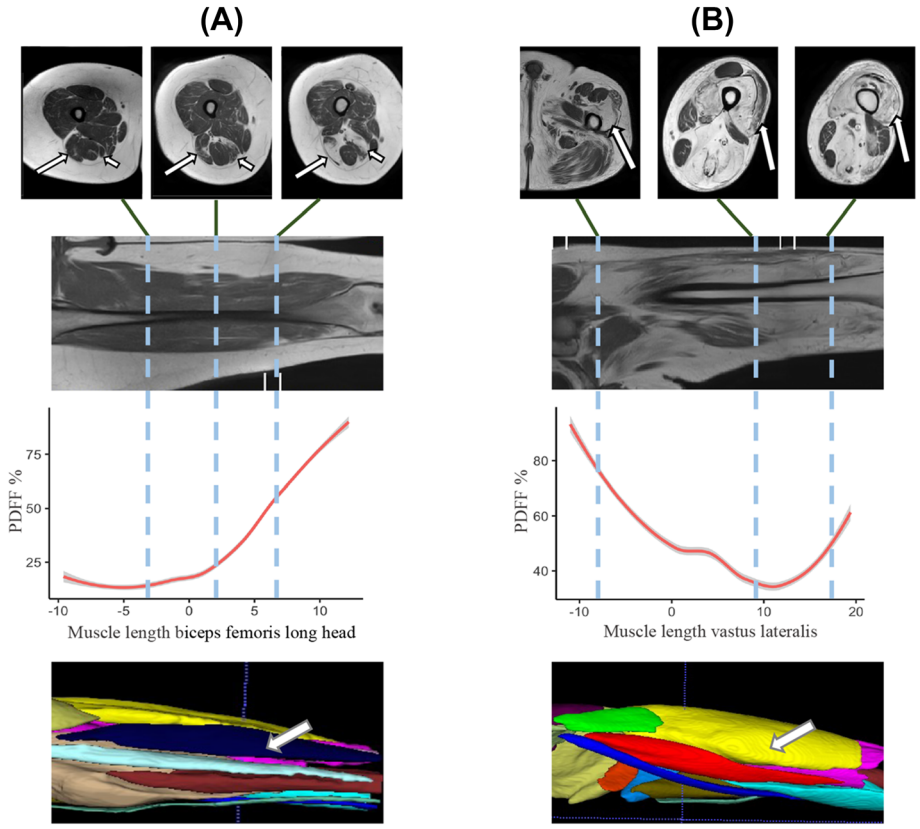

Figure 2 Examples of non-uniform muscle fat replacement in LGMDR12. For two patients (A, B), three axial T1 MRI slices are shown that highlight the non-uniform distribution of muscle fat replacement along the length of individual muscles. The coronal T1 image shows the location of the axial slices. Next, we quantified this non-uniform distribution in the graph displaying the PDFF of the selected muscle along the length of the thigh for this patient. The thickest part of the muscle is centered at '0' on the *x*-axis in centimetres, with the more proximal part of the muscle shown to the left (negative values) and more distal part shown to the right (positive values). Finally, a 3D segmentation model of the thighs is shown, which is used to calculate the PDFF. (A) The biceps femoris long head (long arrows) of the right leg is shown in three different locations along the thigh, highlighting the variation in the degree of fat replacement. The long arrow in the 3D segmentation model also points to this muscle. Short arrows in the axial T1 image point towards the semimembranosus muscle, in which there is also a clear non-uniform fat replacement (not further shown). (B) Long arrows: Vastus lateralis muscle of the left leg.

in comparison with the patient group. These results remained unchanged when the same analysis was done with only the most peripheral, and most central layer of the muscles.

Discussion

Our study showed a strong correlation between PDFF on MRI and fat fraction on muscle biopsy as well as to severity of histopathological changes of the semimembranosus and vastus lateralis muscles in patients with LGMDR12, which supports and validates the use of Dixon MRI in clinical trials. Furthermore, our results demonstrated an inhomogeneous distribution of fat along the length of 18 entire thigh muscles in adult patients with LGMDR12 and healthy controls. We observed that patients often follow a common, muscle-specific pattern of fat replacement, although for some of the most affected muscles in LGMDR12 (e.g., semimembranosus), we detected a large heterogeneity between patients.

MRI fat fraction measurements correlate to muscle biopsy findings

Interestingly, fat fraction was higher on MRI than in corresponding muscle biopsies (Figure 1, A1–3), for which several possible explanations come to mind. First, the measured PDFF depends highly on the MRI device and acquisition parameters, which may explain why in healthy controls in other studies sometimes lower PDFF values are measured.[25]

Second, the methodology and scale of fat fraction analysis on MRI and biopsy inherently differ. Indeed, although the biopsy and MRI are compared at the same level in the muscle, the volumes analysed by each technique are still different. Additionally, fat fraction on MRI and on biopsy

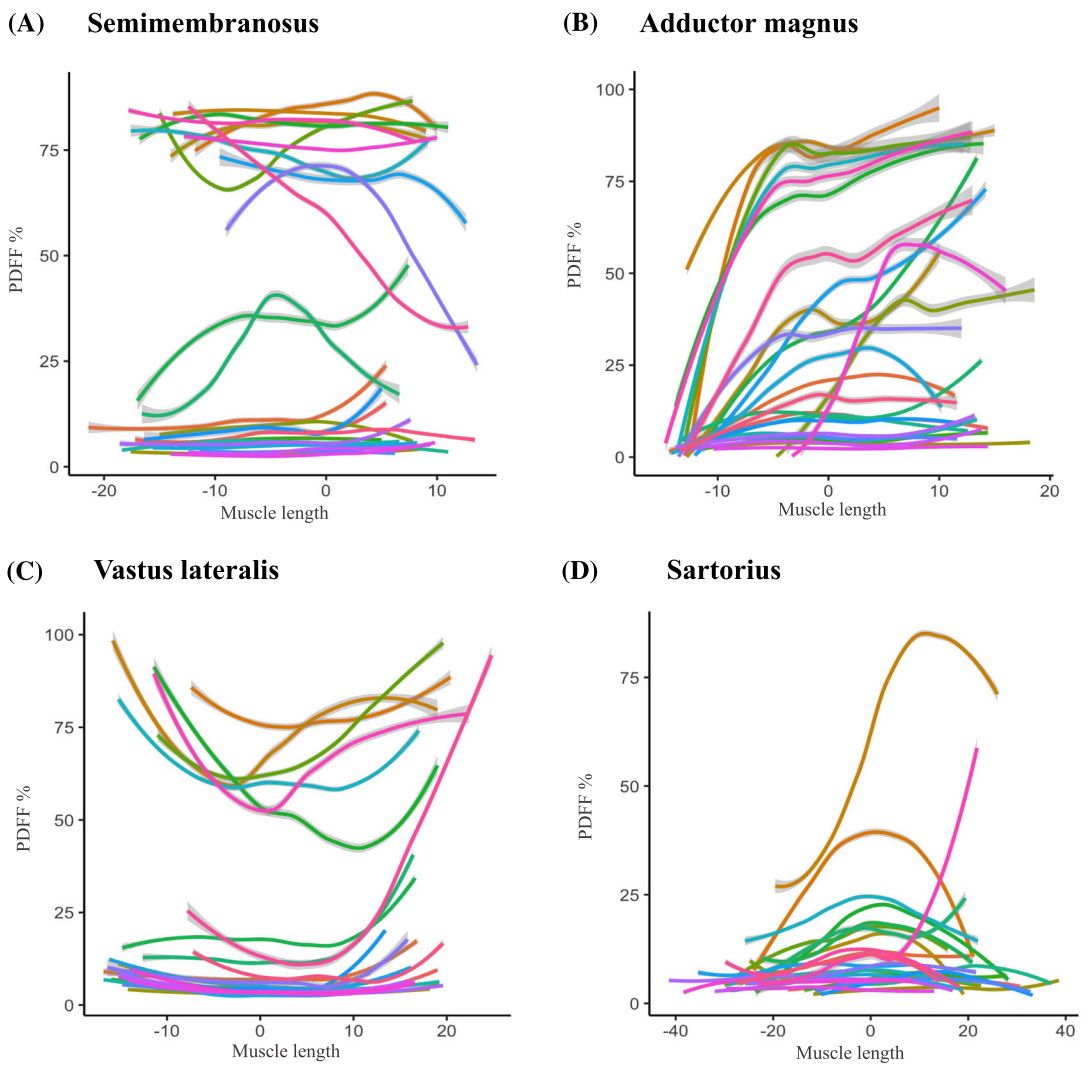

Figure 3 Profiles of muscle fat replacement along the length of thigh muscles in LGMDR12 patients. Four muscles (A–D) are shown for the LGMDR12 patient group that exemplify the range of muscle fat replacement patterns encountered in all thigh muscles: Semimembranosus, adductor magnus, vastus lateralis, and sartorius. (A–D) Each (coloured) line represents the proton density fat fraction (PDFF) of one patient over the length of the muscle from proximal (left side of *x*-axis) to distal (right side of *x*-axis). To display all patients (who have varying thigh lengths) in the same graph, the maximum cross-sectional area (thickest part of the muscle) for each patient is centered at muscle length '0' on the *x*-axis in centimetres, with the more proximal part of the muscle shown to the left (negative values) and more distal part shown to the right (positive values).[7] To aid in visual interpretation, the raw measurement data were smoothed with a generalized additive model (GAM) function with confidence intervals shown as grey bars around the lines, and light grey dashed lines show the 20% and 70% PDFF cut-off. For the semimembranosus (A), the PDFF profile varies greatly between intermediately affected patients. However, for the three other muscles (B–D), we can observe a muscle-specific pattern of fat replacement from proximal to distal that is followed by most patients throughout the different stages of muscle fat replacement.

are intrinsically different measures: the fraction of hydrogen nuclear spins that belong to lipids, and the relative volume occupied by adipose tissue in the biopsy specimen, respectively. There is also the phenomenon of intramyocellular lipids (IMCL), which add to the muscle fat fraction on Dixon MRI (IMCL have been shown to represent approximately 40% of methylene protons in lower leg muscles).[26] This explains the pseudo-overestimation of PDFF by Dixon MRI in healthy controls.

However, the fact that the Bland–Altman analysis showed that the average difference in measured fat fraction on MRI appeared higher in the most affected muscle of patients (semimembranosus) than in controls suggests that these technicalities probably only offer a partial explanation. This might indicate that MRI could detect pathological changes that precede fully formed fat tissue on biopsy, which could be a further argument for its sensitivity as an outcome measure.

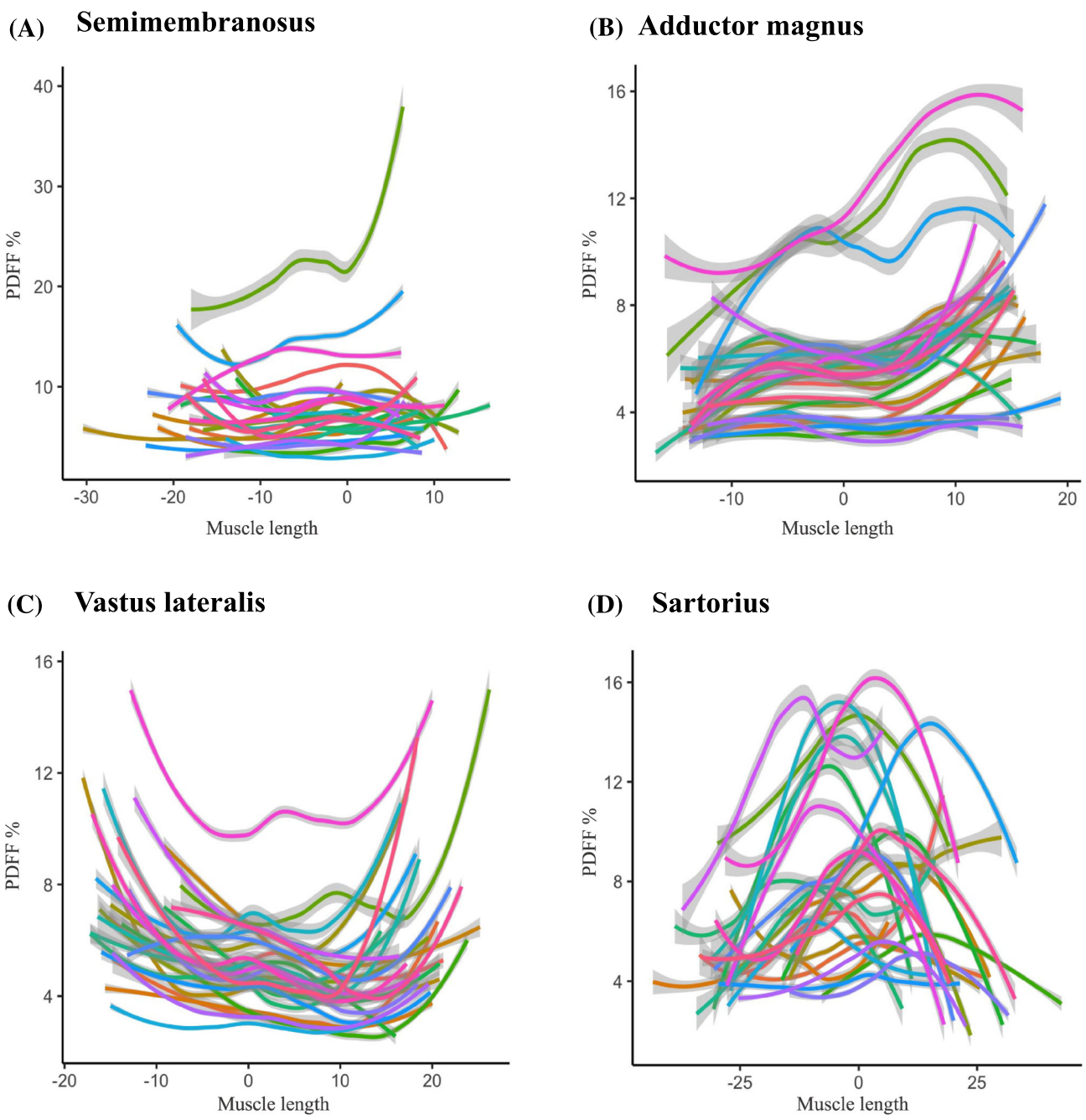

Figure 4 Profiles of PDFF along the length of thigh muscles in healthy controls. The same muscles as in Figure 3 are shown for the control group. Each control individual is indicated in another coloured line. Healthy controls generally show less variation between subjects than patients, with a clearly visible pattern of intramuscular fat distribution for each muscle. Note that this pattern often shows marked similarities with the distribution of fat replacement in LGMDR12 patients.

We did not find a correlation between MRI and biopsy fat percentage in the rectus femoris muscle (which is generally unaffected) in patients or any of the muscles in controls due to the very small dynamic range of the measures. Indeed, in healthy muscles, fat percentage on muscle biopsy bottomed out close to 0% because the biopsy rarely showed any fat tissue, whereas the PDFF on MRI could vary within the normal range of up to 15% as it does in healthy controls. Only two previous other studies directly compared PDFF to muscle biopsy fat fraction.[2,4] The study by Güttsches et al. analysed 10 muscle biopsies in patients with varying neuromuscular disorders, most from the vastus lateralis, and found a similarly strong correlation between Dixon PDFF and biopsy FF. Fat percentage measured on Dixon MRI was also consis-

Table 4 Differences in PDFF between the peripheral and centre half of thigh muscles along the radial axis

Muscles	Patients			Controls			Patients vs. controls
	Mean ± SD	*P*-value	Cohen's *d*	Mean ± SD	*P*-value	Cohen's *d*	*P*-value
Semimembranosus	0.4 ± 2.1	0.135	0.01	0.4 ± 1.1	0.038	0.11	0.877
Biceps femoris long head	0.1 ± 1.7	0.655	<0.01	0.5 ± 1.3	0.080	0.14	0.456
Adductor magnus	0.9 ± 5.1	0.361	0.03	0.8 ± 1.2	0.002	0.37	0.583
Adductor longus	1.0 ± 3.6	0.030	0.04	0.0 ± 0.8	0.943	<0.01	0.048
Semitendinosus	0.5 ± 5.7	0.677	0.02	−2.3 ± 2.5	<**0.001**	0.69	0.078
Vastus medialis	0.2 ± 2.5	0.730	<0.01	0.0 ± 1.2	0.611	<0.01	0.583
Gluteus minimus	−2.2 ± 6.9	0.578	0.09	0.8 ± 1.4	0.002	0.14	0.147
Tensor fascia lata	−0.5 ± 3.3	0.447	0.02	−0.5 ± 2.6	0.058	0.11	0.595
Vastus intermedius	0.5 ± 4.1	0.301	0.02	−0.5 ± 0.9	0.004	0.30	1
Vastus lateralis	−0.9 ± 3.8	0.046	0.04	−0.7 ± 1.1	0.003	0.41	0.640
Biceps femoris short head	−1.8 ± 4.4	0.019	0.08	−2.4 ± 1.8	<**0.001**	0.80	0.959
Gluteus maximus	2.2 ± 2.9	<**0.001**	0.16	1.1 ± 1.1	<**0.001**	0.26	0.089
Adductor brevis	−0.1 ± 2.7	0.077	<0.01	0.6 ± 0.5	<**0.001**	0.52	0.294
Gracilis	2.3 ± 4.8	0.015	0.12	−0.3 ± 1.5	0.594	0.14	0.014
Rectus femoris	1.0 ± 4.9	0.400	0.05	0.4 ± 0.6	**0.001**	0.25	0.426
Gluteus medius	0.3 ± 2.1	0.106	0.03	0.1 ± 1.3	0.604	0.05	0.471
Sartorius	−1.8 ± 3.6	0.004	0.13	−1.6 ± 2.0	<**0.001**	0.41	0.797
Pectineus	−0.4 ± 2.2	0.645	0.04	0.3 ± 0.7	0.053	0.19	0.327

Note: Negative values indicate a higher PDFF in the centre of the muscles as compared with the periphery, and positive values a lower PDFF in the centre. Cohen's effect size is given for each comparison with <0.20 indicating a low effect size and >0.80 a large effect size. The final column shows *P*-values for the comparison of the mean observed differences along the radial axis between the patient and the control groups. Only *P*-values marked in bold remained significant after correction for multiple testing with Holm's stepwise correction.
Abbreviations: PDFF, proton density fat fraction; SD, standard deviation.

tently higher than on muscle biopsy and they concluded that MRI and biopsies correlated mainly in more advanced disease stages. Gaeta et al. analysed 27 biopsies, without specifying from which muscles or differentiating between affected and unaffected muscles, in patients with a wide variety of neuromuscular disorders. Although the applied MRI acquisition and analysis differed, making a direct comparison impossible, they also found a strong correlation between MRI fat fraction and biopsy fat percentage with more similar percentage for both methods.

Fat fraction on MRI was also strongly correlated with the Rochester histopathological grading scale in patients with LGMDR12, which measures other elements such as necrosis and interstitial fibrosis. This is unsurprising, as these pathological changes are an integral part of the disease process of muscular dystrophies next to fat replacement.[27] However, the rectus femoris muscle was again an exception with no such correlation, because often slight histopathological changes were detected despite that all but one of the patients had a PDFF in the normal range. It has been shown that mild histopathological abnormalities are frequently encountered in biopsies of healthy controls, especially with increasing age.[1] This might also be applicable to our results, as we also found a significant correlation between age and rectus femoris histopathology grade in the patients ($\rho = 0.63$, $P = 0.010$). Nevertheless, it might appear that the correlation of Dixon PDFF to biopsy fat percentage or other histopathological changes could be limited to diseased subjects and muscles.

Although inflammation and STIR hyperintensities have already been described in LGMDR12 patients, the co-occurrence of these two phenomena had not yet been previously analysed.[28] STIR hyperintensities indicate an increased muscle water content, which can have many causes such as inflammation, necrosis, denervation, or other forms of oedema.[29] The fact that all muscles with STIR hyperintensities that were biopsied showed inflammatory histopathological changes presents an argument that in the case of LGMDR12 patients, STIR hyperintensities could indicate inflammation. However, a more detailed analysis would be necessary to support this hypothesis, both histologically and radiologically.[30,31] Indeed, T2 water MRI sequences were not part of this study's protocol but should be included in future studies as this would allow the quantification of muscle water content, which is not possible with STIR sequences.

Analysing fat fraction in entire muscles prevents sampling errors

This is the first study to analyse entire thigh muscles from origin to insertion, and our findings have several implications.

Because the PDFF changed significantly along the length of all thigh muscles it is not possible to simply extrapolate the results of an analysis of only a small, arbitrary selection of slices to the entire muscle. Additionally, it is not possible to mathematically correct for this sampling bias because of the non-linear fat replacement patterns.

Some studies attempt to mitigate this issue by selecting 5 non-consecutive slices over a length of up to 13 cm, which is certainly an improvement over single-slice analysis, but largely the same issues remain.[8,32] Indeed, because the pattern of fat replacement varies between muscles, patients

and sometimes disease stages, a selection of 5 slices would approximate the real average PDFF of the analysed muscles better in some muscles and disease stages than others, biasing the results. For example, if only a selection of slices in the central 10–20 cm of the vastus lateralis muscle were analysed, this would incorrectly lead to a lower estimation of the PDFF due to the parabolic shape of fat replacement distribution (Figure 3), and the reverse holds true for the sartorius muscle. Additionally, a risk of error in re-selecting the exact same slices analysed at baseline remains, whereas no such error exists with whole muscle analyses. Indeed, despite several techniques to minimize this error using anatomical reference points or coefficients (e.g., ratio of semimembranosus CSA to semitendinosus CSA) there remains a margin of error in pinpointing the exact analysed slice(s) in consequent MRI scans in longitudinal follow-up studies, which is even further complicated in children who are still growing.[12,14,16] In previous studies, changes in measured PDFF of up to 12% have been reported over as small a distance as 1.5 cm in DMD, and differences of up to 18% over 2.8 cm in LGMDR12, which could obviously confound the measurement of any real progression of muscle fat replacement over a time frame of one year.[7,8]

Of course, trained and motivated technologists are usually able to perform repositioning with an error of <1 cm and up until now many longitudinal MRI studies with a limited number of slices investigated have been successful at describing disease progression despite these limitations, but the increased accuracy of whole muscle analyses will probably further improve on these results in the future. An extra advantage of imaging and analysing entire muscles is the possibility to compare PDFF results more readily between studies, which is currently limited in part because each study analyses different, arbitrarily selected slices of muscles. The reason why only a few slices are typically analysed in the current literature is of course because it is not feasible to manually analyse entire muscles. However, as (semi-)automated muscle segmentation technologies become more widespread, this concern will become irrelevant.

We also showed that when muscles were analysed as groups instead of individually, significant non-uniform muscle fat replacement patterns remain. Consequently, this type of analysis does not average out the heterogeneity encountered in individual muscles and evokes the same concerns.

Finally, but most importantly, we recently showed that muscle sampling not only leads to incorrect estimates of muscle PDFF values, but that it is also less sensitive to measure disease progression in LGMDR12 patients, which directly and negatively affects the performance of this outcome measure in potential clinical trials.[7]

These findings impact research in muscle diseases far beyond LGMDR12, because as long as the distribution of muscle fat replacement in other muscle diseases remains uninvestigated, it cannot be assumed to be homogenous, and sampling small parts of thigh muscles will hold all the biases and associated risks detailed above.[8–11]

Distribution of muscle fat replacement is partially determined by the affected muscle

In Table 3, we listed the patterns of fat replacement followed by most patients and controls for each muscle. It should be noted that these patterns are not as markedly pronounced in every muscle, with some muscles showing more variability between different subjects, and that they can vary depending on disease stage. Nevertheless, despite this variability, fat replacement often appeared to follow a common pattern along the length of specific muscles, which was most pronounced in an intermediate stage of fat replacement but still present in mildly and severely affected muscles. Interestingly, in previous research in children with DMD, a similar distribution of fat replacement along the vastus lateralis muscle was found.[8] In that study, the authors suggested that because the origin and insertion of the muscles experience the greatest stress, these parts are the most susceptible to injury and fat replacement over time. While this hypothesis is certainly plausible, the issue now appears to be more complicated, as we showed that other muscles (e.g., sartorius) have a lower PDFF at their origin and insertion and higher PDFF in the middle. Additionally, this specific distribution pattern of intramuscular fat in these muscles is often already discernible in healthy controls, who should have a normal response to muscle stress (Figures 3 and 4).

Possibly the anatomy of the muscle also plays a role as not all muscles are stressed in the same way (e.g., bi-articular muscles are stressed differently than mono-articular muscles).[33] It was recently also shown that muscles with a longer fibre length and thicker cross-sectional area were preferentially affected in DMD and Becker muscular dystrophy, which could potentially also explain a part of the variation in fat replacement between muscles in other diseases such as LGMDR12.[34] Finally, genetic expression profiles differ greatly between thigh muscles both in LGMDR12 patients and in healthy controls, which might also account for the different severity of involvement and pattern of fat replacement.[17] Further research in other muscle diseases is necessary to evaluate to what extent the pattern of fat replacement along the length of thigh muscles is determined by both the specific muscle characteristics and the underlying disease.

Distribution of intramuscular fat along the radial axis is not different in patients

We showed that although intramuscular fat was not uniformly distributed between the periphery and the centre of

muscles along the radial axis, the differences in PDFF were small and there was considerable variability between patients. Even though it may appear in Table 4 that more muscles in the control group have a significant difference of PDFF along the radial axis than in the patient group, we showed that there was no significant difference between patients and controls for any muscle. The standard deviation of the difference in PDFF along the radial axis for patients was consistently higher than in controls, indicating that on an individual patient level larger fluctuations in the physiological variation are possible, although there was no difference on average. These findings suggest that muscle fat replacement might occur at random locations along the radial axis in LGMDR12, although further research is necessary.

Limitations

Given the cross-sectional nature of this study, we estimate the distribution of muscle fat replacement based on a group of patients with varying ranges of disease severity and duration, as opposed to performing a longitudinal follow-up in individuals. Despite this limitation, the benefit of visualizing patients with varying disease severity and duration in the same graph was that this greatly facilitated the recognition of patterns on a group level. In contrast, longitudinal studies are inherently limited to a couple of years of follow-up, which complicates this. When looking at for example the adductor magnus muscle (Figure 3), one could hypothesize that muscle fat replacement starts distally in the muscle, and gradually advances more proximally in more severely affected patients. Future studies can now use these findings to focus more specifically on confirming these results with a longitudinal study design on an individual level.

Next, because only a minority of patients showed moderately severe fat replacement on muscle biopsies, the reported correlation coefficients could be influenced by outliers, especially in the rectus femoris muscle.

The study had few female patients, which is an accurate representation of the general LGMDR12 population but means that the study results should be interpreted with care in a female population.[35] Finally, because we analysed the radial profile of fat distribution over only a portion (maxCSA) of each muscle, it is possible that we missed radial fat replacement patterns around the origin or insertion of muscles.

In conclusion, we showed that PDFF on MRI correlates strongly to the fat percentage and extent of other histopathological changes on muscle biopsies in adults with LGMDR12. These findings validate the use of Dixon MRI PDFF imaging as an outcome measure in LGMDR12 and further support the broad use of qMRI. We also demonstrated that muscle fat replacement is not homogeneously distributed within thigh muscles of adult LGMDR12 patients, which has important implications for (future) clinical trials. Given the rise of MRI fat fraction imaging as an outcome measure, it is crucial that the PDFF is calculated with minimal biases and maximal accuracy to ensure reliable results. Finally, we discovered that the distribution of intramuscular fat differed between muscles in both the patient and control groups and suggested that this could partially be explained by specific muscle characteristics next to disease specificities.

Acknowledgements

We thank the patients and healthy volunteers for their participation in the study. We are grateful to the technical personnel of the Departments of Radiology and Pathology at UZ Leuven for their valuable support.

Written informed consent was obtained from all participants and the study was approved by the Ethics Committee Research UZ/KU Leuven in accordance with the Declaration of Helsinki. The authors of this manuscript certify that they comply with the ethical guidelines for authorship and publishing in the *Journal of Cachexia, Sarcopenia and Muscle*.[36]

Funding

This study received research funding from the patient organization Association Belge contre les Maladies neuro-Musculaires (ABMM) and the Klinische Onderzoeks-en OpleidingsRaad (KOOR) of University Hospitals Leuven. BDW is supported by the Fund for Scientific Research Flanders (FWO, PhD fellowship fundamental research grant number 1159121N). The work of FM and LH is supported in part by the Internal Funds KU Leuven under Grant C24/18/047 and by the Flemish Government under the "Onderzoeksprogramma Artificiële Intelligentie (AI) Vlaanderen" programme.

Conflict of interest

KGC is Chairholder of the Emil von Behring Chair for Neuromuscular and Neurodegenerative Disorders by CSL Behring. KGC is member of the European Reference Network for Rare Neuromuscular Diseases (ERN EURO-NMD) and of the European Reference Network for Rare Neurological Diseases (ERN-RND). DRT received consultant honorary from GE-Healthcare (UK) and Covance Laboratories (UK), speaker honorary from Novartis Pharma AG (Switzerland), travel reimbursement from GE-Healthcare (UK) and UCB (Belgium) and collaborated with Novartis Pharma AG (Switzerland),

Probiodrug (Germany), GE-Healthcare (UK), and Janssen Pharmaceutical Companies (Belgium), none related to the work in this paper. The authors report no disclosures relevant to the manuscript.

Online supplementary material

Additional supporting information may be found online in the Supporting Information section at the end of the article.

References

1. Lassche S, Küsters B, Heerschap A, Schyns MVP, Ottenheijm CAC, Voermans NC, et al. Correlation Between Quantitative MRI and Muscle Histopathology in Muscle Biopsies from Healthy Controls and Patients with IBM, FSHD and OPMD. *J Neuromuscul Dis* 2020;**7**:495–504.
2. Güttsches AK, Rehmann R, Schreiner A, Rohm M, Forsting J, Froeling M, et al. Quantitative Muscle-MRI Correlates with Histopathology in Skeletal Muscle Biopsies. *J Neuromuscul Dis* 2021;**8**:669–678.
3. Kinali M, Arechavala-Gomeza V, Cirak S, Glover A, Guglieri M, Feng L, et al. Muscle histology vs MRI in Duchenne muscular dystrophy. *Neurology* 2011;**76**:346–353.
4. Gaeta M, Scribano E, Mileto A, Mazziotti S, Rodolico C, Toscano A, et al. Muscle fat fraction in neuromuscular disorders: dual-echo dual-flip-angle spoiled gradient-recalled MR imaging technique for quantification - a feasibility study. *Radiology* 2011;**259**: 487–494.
5. Burakiewicz J, Sinclair CDJ, Fischer D, Walter GA, Kan HE, Hollingsworth KG. Quantifying fat replacement of muscle by quantitative MRI in muscular dystrophy. *J Neurol* 2017;**264**:2053–2067.
6. Bolduc V, Marlow G, Boycott KM, Saleki K, Inoue H, Kroon J, et al. Recessive mutations in the putative calcium-activated chloride channel Anoctamin 5 cause proximal LGMD2L and distal MMD3 muscular dystrophies. *Am J Hum Genet* 2010;**86**: 213–221.
7. De Wel B, Huysmans L, Peeters R, Goosens V, Ghysels S, Byloos K, et al. Prospective Natural History Study in 24 Adult Patients With LGMDR12 Over 2 Years' Follow-up: Quantitative MRI and Clinical Outcome Measures. *Neurology* 2022;**99**:e638–e649.
8. Hooijmans MT, Niks EH, Burakiewicz J, Anastasopoulos C, van den Berg SI, van Zwet E, et al. Non-uniform muscle fat replacement along the proximodistal axis in Duchenne muscular dystrophy. *Neuromuscul Disord* 2017;**27**:458–464.
9. Greve T, Burian E, Zoffl A, Feuerriegel G, Schlaeger S, Dieckmeyer M, et al. Regional variation of thigh muscle fat infiltration in patients with neuromuscular diseases compared to healthy controls. *Quant Imaging Med Surg* 2021;**11**: 2610–2621.
10. Gaeta M, Mileto A, Mazzeo A, Minutoli F, di Leo R, Settineri N, et al. MRI findings, patterns of disease distribution, and muscle fat fraction calculation in five patients with Charcot-Marie-Tooth type 2 F disease. *Skeletal Radiol* 2012;**41**:515–524.
11. Janssen BH, Voet NBM, Nabuurs CI, Kan HE, de Rooy JWJ, Geurts AC, et al. Distinct Disease Phases in Muscles of Facioscapulohumeral Dystrophy Patients Identified by MR Detected Fat Infiltration. *PLoS ONE* 2014;**9**:e85416.
12. Fischmann A, Morrow JM, Sinclair CDJ, Reilly MM, Hanna MG, Yousry T, et al. Improved anatomical reproducibility in quantitative lower-limb muscle MRI. *J Magn Reson Imaging* 2014;**39**:1033–1038.
13. Fischmann A, Hafner P, Fasler S, Gloor M, Bieri O, Studler U, et al. Quantitative MRI can detect subclinical disease progression in muscular dystrophy. *J Neurol* 2012;**259**: 1648–1654.
14. Willis TA, Hollingsworth KG, Coombs A, Sveen ML, Andersen S, Stojkovic T, et al. Quantitative Muscle MRI as an Assessment Tool for Monitoring Disease Progression in LGMD2I: A Multicentre Longitudinal Study. *PLoS ONE* 2013;**8**:e70993.
15. Bonati U, Hafner P, Schädelin S, Schmid M, Naduvilekoot Devasia A, Schroeder J, et al. Quantitative muscle MRI: A powerful surrogate outcome measure in Duchenne muscular dystrophy. *Neuromuscul Disord* 2015;**25**:679–685.
16. Murphy AP, Morrow J, Dahlqvist JR, Stojkovic T, Willis TA, Sinclair CDJ, et al. Natural history of limb girdle muscular dystrophy R9 over 6 years: searching for trial endpoints. *Ann Clin Transl Neurol* 2019;1033–1045.
17. Depuydt CE, Goosens V, Janky R, D'Hondt A, De Bleecker JL, Noppe N, et al. Unraveling the Molecular Basis of the Dystrophic Process in Limb-Girdle Muscular Dystrophy LGMD-R12 by Differential Gene Expression Profiles in Diseased and Healthy Muscles. *Cell* 2022;**11**:1508.
18. Yushkevich P, Piven J, Hazlett H. User-guided 3D active contour segmentation of anatomical structures: significantly improved efficiency and reliability. *Neuroimage* 2006;**31**:1116–1128.
19. Statland JM, Shah B, Henderson D, van der Maarel S, Tapscott SJ, Tawil R. Muscle pathology grade for facioscapulohumeral muscular dystrophy biopsies. *Muscle Nerve* 2015;**52**:521–526.
20. Liu CY, McKenzie CA, Yu H, Brittain JH, Reeder SB. Fat quantification with IDEAL gradient echo imaging: Correction of bias from T1 and noise. *Magn Reson Med* 2007;**58**:354–364.
21. Ronneberger O, Fischer P, Brox T. U-Net: Convolutional Networks for Biomedical Image Segmentation. *Lect Notes Comput Sci* 2015;**9351**:234–241.
22. Burnham KP, Anderson DR. *Multimodel Inference: Understanding AIC and BIC in Model Selection*. Vol. **33**; 2016. p. 261–304. https://doi.org.kuleuven.e-bronnen.be/101177/0049124104268644
23. Molenberghs G, Verbeke G. *Linear Mixed Models for Longitudinal Data*. Published Online First: 2000.
24. Holme S. A Simple Sequentially Rejective Multiple Test Procedure. *Scand J Stat* 1979;**6**:65–70.
25. Morrow JM, Sinclair CDJ, Fischmann A, Reilly MM, Hanna MG, Yousry TA, et al. Reproducibility, and age, body-weight and gender dependency of candidate skeletal muscle MRI outcome measures in healthy volunteers. *Eur Radiol* 2014;**24**:1610–1620.
26. Torriani M, Thomas BJ, Bredella MA, Ouellette H. Intramyocellular lipid quantification: comparison between 3.0- and 1.5-T (1)H-MRS. *Magn Reson Imaging* 2007;**25**: 1105–1111.
27. Smith LR, Barton ER. Regulation of fibrosis in muscular dystrophy. *Matrix Biol* 2018; **68–69**:602–615.
28. Holm-Yildiz S, Witting N, de Stricker Borch J, Kass K, Khawajazada T, et al. Muscle biopsy and MRI findings in ANO5-related myopathy. *Muscle Nerve* 2021;**64**:743–748.
29. Dahlqvist JR, Widholm P, Leinhard OD, Vissing J. MRI in Neuromuscular Diseases: An Emerging Diagnostic Tool and Biomarker for Prognosis and Efficacy. *Ann Neurol* 2020;**88**:669–681.
30. Tasca G, Pescatori M, Monforte M, Mirabella M, Iannaccone E, Frusciante R, et al. Different Molecular Signatures in Magnetic Resonance Imaging-Staged Facioscapulohumeral Muscular Dystrophy Muscles. *PLoS ONE* 2012;**7**:e38779.
31. Paoletti M, Pichiecchio A, Piccinelli SC, Tasca G, Berardinelli AL, Padovani A, et al. Advances in quantitative imaging of genetic and acquired myopathies: Clinical applications and perspectives. *Front Neurol* 2019;**10**:1–21.
32. Reyngoudt H, Marty B, Boisserie J-M, le Louër J, Koumako C, Baudin PY, et al. Global versus individual muscle segmentation to assess quantitative MRI-based fat fraction changes in neuromuscular diseases. *Eur Radiol* 2021;**31**:4264–4276.
33. van Ingen Schenau GJ, Bobbert MF, Rozendal RH. The unique action of bi-articular muscles in complex movements. *J Anat* 1987;**155**:1.
34. Veeger TTJ, van Zwet EW, al Mohamad D, Naarding KJ, van de Velde NM, Hooijmans MT, et al. Muscle architecture is associated with muscle fat replacement in Duchenne

and Becker muscular dystrophies. *Muscle Nerve* 2021;**64**:576–584.
35. Hicks D, Sarkozy A, Muelas N, Koehler K, Huebner A, Hudson G, et al. A founder mutation in Anoctamin 5 is a major cause of limb girdle muscular dystrophy. *Brain* 2011;**134**:171–182.
36. von Haehling S, Morley JE, Coats AJS, Anker SD. Ethical guidelines for publishing in the Journal of Cachexia, Sarcopenia and Muscle: update 2021. *J Cachexia Sarcopenia Muscle* 2021;**12**:2259–2261.